β decay study of ^{168}Hf and a test of new geometrical models

E. A. McCutchan,[1] R. F. Casten,[1] V. Werner,[1] A. Wolf,[2] Z. Berant,[2] R. J. Casperson,[1] A. Heinz,[1] R. Lüttke,[1,3] B. Shoraka,[1,4] J. R. Terry,[1] E. Williams,[1] and R. Winkler[1]

[1]*WNSL, Yale University, New Haven, Connecticut 06520, USA*
[2]*Nuclear Research Center Negev, Beer-Sheva 84190, Israel*
[3]*Technische Universität Darmstadt, D-64289 Darmstadt, Germany*
[4]*Department of Physics, University of Surrey, Guildford, Surrey GU2 7XH, United Kingdom*

(Received 30 July 2007; published 6 December 2007)

Excited low-spin, nonyrast states of ^{168}Hf were populated in β^+/ϵ decay and studied through γ-ray spectroscopy to assess the nature of low-lying $K^\pi = 0^+, 2^+$ intrinsic excitations. Coincidence data provided improved measurements of the decay properties of the low-lying states, and γ-γ angular correlation measurements yielded spin assignments for several levels as well as $E2/M1$ mixing ratios. The resulting level scheme of ^{168}Hf is compared with the predictions of new simple geometrical models, including the confined beta soft model and the Davidson potential. It is found that the predictions for most observables are similar for all the models and in agreement with the data on ^{168}Hf. However, large differences exist in the predictions for the excited $K = 0^+$ sequence, with the Davidson potential best reproducing the data in ^{168}Hf.

DOI: 10.1103/PhysRevC.76.064307 PACS number(s): 21.10.Re, 23.20.Lv, 21.60.Ev, 27.70.+q

I. INTRODUCTION

The available methods for modeling transitional to axially symmetric deformed nuclei have undergone a renaissance in recent years. Traditionally, these nuclei have been described by models incorporating multiparameter Hamiltonians, such as the interacting boson approximation (IBA) [1] or the geometric collective model (GCM) [2–4]. Now, new models based on a geometrical perspective are emerging that provide single-parameter predictions for structure spanning transitional to axially symmetric deformed. The underlying idea behind each of these models is to make use of a simple potential in the Bohr Hamiltonian, yielding analytic solutions for both energies and electromagnetic transition strengths.

From a theoretical perspective, analytic solutions to the Bohr Hamiltonian are interesting in themselves. Still, it can also be explored to what extent these simple potentials provide realistic descriptions of actual nuclei. In the present work, an experimental study of ^{168}Hf is presented to test the predictions of some of these new geometrical models. Most models more or less converge to similar values (as they approach the rigid-rotor limit) in their predictions for very well deformed nuclei. However, predictions for several properties of the excited $K = 0^+$ excitations are dramatically different for less deformed structures. Since ^{168}Hf, with a ground state $R_{4/2} \equiv E(4_1^+)/E(2_1^+)$ of 3.11, is situated in a region outside of well-deformed structures, it should provide a good test case for determining the applicability of different geometrical models.

The models appropriate for describing ^{168}Hf include the confined beta soft (CBS) model [5], the Davidson potential [6,7], and the exactly separable version of the Davidson potential [8]. The starting point for all of these models is the original Bohr Hamiltonian [9]

$$H = -\frac{\hbar^2}{2B}\left[\frac{1}{\beta^4}\frac{\partial}{\partial\beta}\beta^4\frac{\partial}{\partial\beta} + \frac{1}{\beta^2\sin 3\gamma}\frac{\partial}{\partial\gamma}\sin 3\gamma\frac{\partial}{\partial\gamma} - \frac{1}{4\beta^2}\sum_{k=1,2,3}\frac{Q_k^2}{\sin^2\left(\gamma - \frac{2}{3}\pi k\right)}\right] + V(\beta,\gamma), \quad (1)$$

where β and γ are the usual collective coordinates, Q_k ($k = 1, 2, 3$) are the components of angular momentum in the intrinsic frame, and B is the mass parameter. Each of these models incorporates a harmonic oscillator potential in the γ degree of freedom (with a minimum at $\gamma = 0^\circ$) and is characterized by a specific potential in the β degree of freedom. The CBS model [5] incorporates an infinite square well potential in the β deformation, where the position of the inner wall can be varied. The localization of the potential is given by a single parameter, $r_\beta = \beta_m/\beta_M$, where $\beta_m(\beta_M)$ gives the position of the inner (outer) wall of the infinite well. A schematic potential for the CBS model is illustrated in Fig. 1(a). The parameter r_β can be varied between 0 and 1, which describes structure between the limits of X(5) [10] and the rigid rotor, respectively. Thus, the CBS model can be applied to describe nuclei with $R_{4/2}$ values ranging from 2.90($r_\beta = 0$) through 3.33 ($r_\beta = 1$).

The Davidson potential [6] is of the form

$$V(\beta) = \beta^2 + \frac{\beta_o^4}{\beta^2}, \quad (2)$$

where the single free parameter (aside from scale) is β_o, which gives the position of the minimum of the potential in β. Examples of the Davidson potential for a few values of the parameter β_o are given in Fig. 1(b). The parameter β_o can, in theory, range from 0 to infinity. For $\beta_o = 0$, the Davidson potential predicts $R_{4/2} = 2.65$. Significantly large values of β_o are not required to reach the rigid-rotor limit: For example, with $\beta_o = 4.0$, the Davidson potential predicts $R_{4/2} = 3.32$.

In the original formulation of the CBS model and the Davidson potential, the separation of the β and γ variables is approximate. An exact separation of variables can be achieved by considering related potentials of the form

$$u(\beta,\gamma) = u(\beta) + \frac{u(\gamma)}{\beta^2}. \quad (3)$$

Taking the potential in the γ degree of freedom to be of harmonic oscillator form, $u(\gamma) = (3c^2)\gamma^2/2$, and $u(\beta)$ as

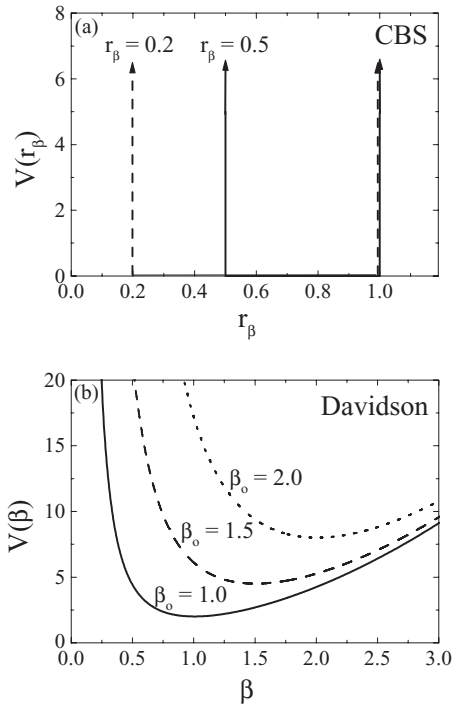

FIG. 1. Potentials in the β degree of freedom used in (a) the CBS model and (b) the Davidson potential. In both cases, the potential is given in arbitrary units. The r_β values given in the plot for the CBS model are specific values for which the CBS predictions are discussed in the text.

the Davidson potential gives the so-called exactly separable Davidson (ES-D) model [7]. This model incorporates two free parameters, β_o and c, where c is a measure of the stiffness of the potential in the γ degree of freedom.

The predictions of the CBS model and the Davidson potential include the ground-state band and excited $K = 0^+$ excitations. The exactly separable version of the Davidson potential also includes predictions for $K = 2^+$ excitations. Although such states are rather well studied in well-deformed nuclei ($R_{4/2} > 3.2$), less information is known in the more transitional region, $R_{4/2} = 2.9$–3.2.

To appropriately test the validity of these models, additional data are required on transitional nuclei. The present work makes use of high-statistics, γ-ray coincidence data, leading to a substantial revision of the previous ^{168}Hf level scheme and improved measurements of intensities of low-lying transitions. In addition, the present work includes measurements of γ-γ angular correlations to obtain $E2/M1$ mixing ratios for transitions between low-lying states and to make definite spin assignments.

II. β-DECAY SPECTROSCOPY EXPERIMENT

Low-spin states in ^{168}Hf were populated in the β^+/ϵ decay of ^{168}Ta and studied through off-beam γ-ray spectroscopy. The parent ^{168}Ta nuclei were produced through the ^{159}Tb(^{16}O, $7n$) reaction by bombarding a $\sim$4.4-mg/cm^2 target with a $\sim$2-pnA, 130-MeV ^{16}O beam provided by the Yale ESTU

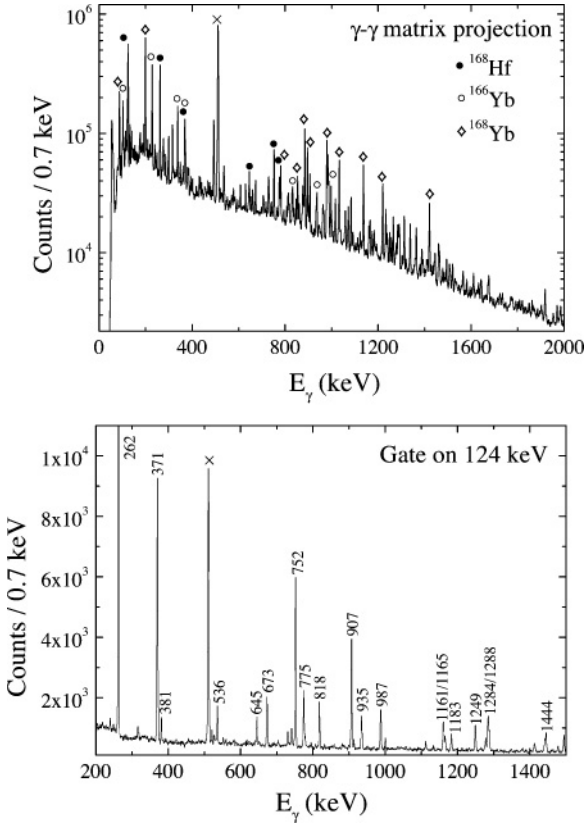

FIG. 2. (Top) Projection of Clover-Clover coincidence matrix. Intense transitions from ^{168}Hf (solid circles), ^{166}Yb (open circles), ^{168}Yb (open diamonds), and 511-keV annihilation radiation (cross) are marked. (Bottom) Spectrum gated on the 124-keV, $2_1^+ \rightarrow 0_1^+$ transition in ^{168}Hf. Intense transitions belonging to ^{168}Hf are labeled by their energy in keV.

tandem accelerator. The experiment was performed with a beam-on/beam-off cycle of 20-s intervals.

During the beam-off cycle, γ rays were detected using eight Compton-suppressed segmented YRAST Ball Clover HPGe detectors [11]. Both γ-ray singles and γ-γ coincidence data were acquired in event mode. The experiment yielded 7.6×10^7 Clover-Clover coincidence events and 1.0×10^7 Clover singles events. The γ-γ projected spectrum is shown in Fig. 2(top). In addition to ^{168}Hf, significant contributions from ^{166,168}Yb are also observed. Figure 2(bottom) illustrates a gate on the 124-keV, $2_1^+ \rightarrow 0_1^+$ transition in ^{168}Hf, showing that mainly only lines from ^{168}Hf are observed in the gated spectrum.

The level scheme for ^{168}Hf obtained in the present work provided a substantial modification to the current literature β^+/ϵ decay data [12] on ^{168}Hf. No evidence is found for two levels previously proposed in β decay. Fifteen new levels are identified and the decay properties of several levels are substantially modified. Table I summarizes the γ rays assigned to ^{168}Hf based on γ-γ coincidences from the present experiment, including their placements, intensities, and the most useful coincidence relations. Table II lists the levels populated in ^{168}Hf and their γ decay. Intensity limits for spin-allowed but unobserved transitions between levels

TABLE I. Observed γ-ray transitions in ^{168}Hf, arranged in order of increasing transition energy. Relative (in β decay) intensities (normalized to $I_{124} \equiv 100$) and the most useful coincidence relations are given.

E_γ (keV)	E_i (keV)	E_f (keV)	I_γ	Coincidences[a]
124.10(5)	124.10	0.00	100(3)	262, 371, 752, 818, 907, 935, 1161, 1249
261.85(5)	385.95	124.10	63.2(18)	124, 371, 645, 673, 775, 987
370.62(8)[b]	1401.58	1030.95	1.9(2)	124, 262, 645, 907
371.36(6)	757.31	385.95	4.0(4)	124, 262, 527, 629, 740
380.88(8)[b]	1411.78	1030.95	1.7(2)	124, 262, 645, 907
390.65(10)[b]	1551.39	1160.76	0.33(3)	124, 262, 775
520.5(1)[b]	1551.39	1030.95	1.5(3)	124, 262, 645, 907
525.6(1)[b]	1401.58	875.90	0.86(12)	124, 752, 876
527.4(1)[c]	1284.65	757.31	0.88(11)	124, 262, 371
535.88(7)[b]	1411.78	875.90	7.8(6)	124, 752, 876
559.4(1)[b]	1618.05	1058.65	0.68(8)	124, 262, 673, 935, 1059
612.8(1)[b]	1671.5	1058.65	0.95(9)	124, 262, 673, 935, 1059
629.1(1)[b]	1386.41	757.31	0.47(6)	124, 262, 371
640.5(1)[b]	1671.5	1030.95	0.90(10)	124, 262, 645, 907
645.05(10)[c]	1030.95	385.95	2.6(3)	124, 262, 371, 381, 521, 641, 1322
672.75(8)	1058.65	385.95	7.2(6)	124, 262, 559, 613
729.3(1)[b]	1671.5	942.07	0.69(9)	124, 818
739.98(11)[b]	1497.25	757.31	0.83(10)	124, 262, 371
742.0(1)[b]	1618.05	875.90	1.9(2)	124, 752, 876
751.81(8)	875.90	124.10	23.0(18)	124, 526, 536, 742, 795, 858, 876, 1477
774.80(9)	1160.76	385.95	9.7(9)	124, 262, 391, 887
795.4(2)[b]	1671.5	875.90	0.76(9)	124, 752, 876
817.98(7)	942.07	124.10	6.4(7)	124, 729
858.03(8)[b]	1733.97	875.90	1.1(1)	124, 752, 876
875.95(9)	875.90	0.00	12.8(5)	526, 536, 742, 795, 858, 876, 1477
887.2(1)[d]	2047.9	1160.76	0.23(5)	124, 775
898.8(2)[c]	1284.65	385.95	0.42(8)	124, 262
906.81(7)	1030.95	124.10	17.7(14)	124, 371, 381, 521, 641, 1322
934.51(10)	1058.65	124.10	6.0(6)	124, 559, 613
987.21(9)	1373.11	385.95	8.4(7)	124, 262
1000.46(9)[b]	1386.41	385.95	1.9(2)	124, 262
1058.60(10)	1058.65	0.00	11.8(8)	559, 613
1111.29(8)[b]	1497.25	385.95	1.8(2)	124, 262
1160.5(1)	1284.65	124.10	5.6(7)	124
1165.4(1)[b]	1551.39	385.95	3.0(4)	124, 262
1182.57(8)	1568.52	385.95	4.0(3)	124, 262
1248.98(10)	1373.11	124.10	5.7(6)	124
1277.4(1)[b]	1401.58	124.10	2.7(3)	124
1284.2(1)	1408.28	124.10	7.1(8)	124
1287.7(2)[b]	1411.78	124.10	4.1(5)	124
1322.0(1)[b]	2352.0	1030.95	0.42(8)	124, 262, 645, 907
1348.1(1)[b]	1733.97	385.95	0.56(7)	124, 262
1411.4(2)[e]	1797.2	385.95	1.0(3)	124, 262
1413.5(2)[e]	1799.5	385.95	1.8(4)	124, 262
1444.42(10)	1568.52	124.10	4.3(4)	124
1477.2(1)[b]	2352.0	875.90	0.72(13)	124, 752, 876
1493.92(8)[b]	1618.05	124.10	4.0(3)	124
1520.1(1)[d]	1644.2	124.10	2.9(3)	124
1580.7(1)[d]	1966.7	385.95	0.95(12)	124, 262
1610.0(1)[b]	1733.97	124.10	2.4(4)	124
1673.0(2)[e]	1797.2	124.10	0.7(2)	124
1675.5(2)[e]	1799.5	124.10	3.0(7)	124
1722.8(1)[b]	2108.6	385.95	0.5(1)	124, 262
1984.5(2)[b]	2108.6	124.10	1.4(3)	124

[a]Only those coincident transitions most relevant to the placement of the tabulated transition or to measurement of its intensity are listed. For low-lying transitions coincident with a large number of feeding transitions, the weaker feeding transitions are omitted.

[b]γ-ray line was not previously reported [12].

[c]γ-ray line was observed in Ref. [13], but not in Ref. [14].

[d]Placement of transition is tentative.

[e]Transitions from the closely spaced levels at 1797.2 and 1799.5 keV are most likely doublets. Each transition is assigned a primary placement as depopulating one of these levels on the basis of the transition energy measured in a gated spectra but may contain an unresolved contribution from the other depopulating member of the pair.

relevant to the structural interpretation of ^{168}Hf are included for some low-lying levels. In the tables and the following discussion, intensities are normalized to the intensity of the 124-keV, $2_1^+ \rightarrow 0_1^+$ transition ($I_{124} \equiv 100$) in ^{168}Hf, except where noted. The level scheme deduced in the present work for levels below 1800 keV is given in Fig. 3.

We also constructed γ-γ angular correlations using the YRAST Ball array recently reconfigured to have the Compton-suppressed Clover detectors positioned at angles appropriate for angular distribution and correlation measurements. More details on the setup will follow in a subsequent publication. The Clover detectors were positioned at relative angles of 180°, 48.5°, 97°, and 90°, equivalent for angular correlation analysis to first-quadrant angles of 0°, 48.5°, 83°, and 90°, respectively. The angular correlation measurements were first tested by measuring correlations with pure multipolarities. Figure 4 illustrates the correlations of three such cascades: 262–124 keV ($4_1^+ \rightarrow 2_1^+ \rightarrow 0_1^+$) and 818–124 keV ($0_2^+ \rightarrow 2_1^+ \rightarrow 0_1^+$) in ^{168}Hf and 228–102 keV ($4_1^+ \rightarrow 2_1^+ \rightarrow 0_1^+$) in ^{166}Yb. The coefficients a_2 and a_4 in Fig. 4 are not corrected for solid angle attenuation. The coefficients A_2 and A_4, after application

TABLE II. Levels populated in ^{168}Hf and their γ decay. Intensities are given for γ-ray transitions depopulating the levels and compared with literature values [12] where available. Intensity limits are given for spin-allowed but unobserved transitions between low-lying levels relevant to the structural interpretation of the nucleus. For these limits, the approximate transition energy expected from the level energy difference is shown in brackets. For levels above 1300 keV, the tentative spin assignments are based on observed transitions to levels of known spin.

J_i^π	E_i (keV)	J_f^π	E_f (keV)	E_γ (keV)	I_γ	$I_{\gamma\text{lit}}$[a]	I_γ^{rel}	$I_{\gamma\text{lit}}^{\text{rel}}$
2^+	124.10(5)	0^+	0.00	124.10(5)	100(3)	100(4)	100(3)	100(4)
4^+	385.95(6)	2^+	124.10	261.85(5)	63.2(18)	63.7(21)	100(3)	100(3)
6^+	757.31(6)	4^+	385.95	371.36(6)	4.0(4)	11.7(9)	100(3)	100(8)
2^{+}[b]	875.90(8)	0^+	0.00	875.95(9)	12.8(5)	12.7(20)	55.7(22)	62(10)
		2^+	124.10	751.81(8)	23.0(18)	20.6(16)	100(8)	100(8)
		4^+	385.95	[490]	<0.10			
0^{+}[b]	942.07(8)	2^+	124.10	817.98(7)	6.4(7)	5.8(17)	100(11)	100(30)
3^{+}[b]	1030.95(7)	2^+	124.10	906.81(7)	17.7(14)	13.9(10)	100(8)	100(7)
		4^+	385.95	645.05(10)[c]	2.6(3)	8.5(14)[d], <3[e]	15(2)	61(10)[d], <22[e]
2^{+}[b]	1058.65(10)	0^+	0.00	1058.60(10)	11.8(8)	9.8(23)	100(7)	100(23)
		2^+	124.10	934.51(10)	6.0(6)	7.4(13)	51(5)	76(13)
		4^+	385.95	672.75(8)	7.2(6)	7.0(19)	61(5)	71(19)
		2^+	875.90	[183]	<0.10			
		0^+	942.07	[117]	<0.20			
4^{+}[b]	1160.76(10)	2^+	124.10	[1037]	<0.30			
		4^+	385.95	774.80(9)	9.7(9)	7.8(20)	100(9)	100(25)
		6^+	757.51	[403]	<0.1			
		2^+	875.90	[285]	<0.2			
		3^+	1030.95	[130]	<0.25			
4^+	1284.65(15)	2^+	124.10	1160.5(1)	5.6(7)	5.7(30)	100(13)	100(53)
		4^+	385.95	898.8(2)[c]	0.42(8)	5.4(11)[d], <3.7[e]	7.5(14)	95(20)[d], <66[e]
		6^+	757.31	527.4(1)[c]	0.88(11)	7.3(8)[d], <2.5[e]	16(2)	128(14), <44[e]
		2^+	875.90	[409]	<0.10			
		2^+	1058.65	[226]	<0.40			
(2, 3, 4)	1373.11(12)	2^+	124.10	1248.98(10)	5.7(6)	6.4(20)	68(7)	58(18)
		4^+	385.95	987.21(9)	8.4(7)	11.1(22)	100(8)	100(20)
(4, 5, 6)	1386.41(9)[f]	4^+	385.95	1000.46(9)[g]	1.9(2)		100(11)	
		6^+	757.31	629.1(1)[g]	0.47(6)		25(3)	
	1401.58(9)[f]	2^+	124.10	1277.4(1)[g]	2.7(3)		100(11)	
		2^+	875.90	525.6(1)[g]	0.86(12)		32(5)	
		3^+	1030.95	370.62(8)[g]	1.9(2)		70(7)	
	1408.28(10)	2^+	124.10	1284.2(1)	7.1(8)	7.2(20)	100(11)	100(28)
	1411.78(8)[f]	2^+	124.10	1287.7(2)[g]	4.1(5)		53(6)	
		2^+	875.90	535.88(7)[g]	7.8(6)		100(8)	
		3^+	1030.95	380.88(8)[g]	1.7(2)		22(3)	
(4, 5, 6)	1497.25(12)[f]	4^+	385.95	1111.29(8)[g]	1.8(2)		100(11)	
		6^+	757.31	739.98(11)[g]	0.83(10)		46(5)	
	1551.39(14)[f]	4^+	385.95	1165.4(1)[g]	3.0(4)		100(13)	
		3^+	1030.95	520.5(1)[g]	1.5(3)		50(10)	
		4^+	1160.76	390.65(10)[g]	0.33(3)		11(1)	
(2, 3, 4)	1568.52(8)	2^+	124.10	1444.42(10)	4.3(4)	2.7(10)	100(9)	100(37)
		4^+	385.95	1182.57(8)	4.0(3)	4.6(31)	93(7)	170(115)
	1618.05(15)[f]	2^+	124.10	1493.92(8)[g]	4.0(3)		100(8)	
		2^+	875.90	742.0(1)[g]	1.9(2)		48(5)	
		2^+	1058.65	559.4(1)[g]	0.68(8)		17(2)	
	1644.2(1)[h]	2^+	124.10	1520.1(1)[g,i]	2.9(3)		100(10)	
(2^+)	1671.5(1)[f]	2^+	875.90	795.4(2)[g]	0.76(9)		80(9)	
		0^+	942.07	729.3(1)[g]	0.69(9)		73(10)	
		3^+	1030.95	640.5(1)[g]	0.90(10)		95(11)	
		2^+	1058.65	612.8(1)[g]	0.95(9)		100(9)	
(2, 3, 4)	1733.97(15)[f]	2^+	124.10	1610.0(1)[g]	2.4(4)		100(7)	
		4^+	385.95	1348.1(1)[g]	0.56(7)		23(3)	
		2^+	875.90	858.03(8)[g]	1.1(1)		46(4)	

TABLE II. *(Continued.)*

J_i^π	E_i (keV)	J_f^π	E_f (keV)	E_γ (keV)	I_γ	$I_{\gamma\text{lit}}$[a]	I_γ^{rel}	$I_{\gamma\text{lit}}^{\text{rel}}$
(2, 3, 4)	1797.2(2)[f]	2^+	124.10	1673.0(2)[g,j]	0.7(2)		70(20)	
		4^+	385.95	1411.4(2)[g,j]	1.0(3)		100(30)	
(2, 3, 4)	1799.5(2)[f]	2^+	124.10	1675.5(2)[g,j]	3.0(7)		100(23)	
		4^+	385.95	1413.5(2)[g,j]	1.8(4)		60(13)	
	1966.7(1)[h]	4^+	385.95	1580.7(1)[g,i]	0.95(12)		100(13)	
	2047.9(2)[h]	4^+	1160.76	887.2(1)[g,i]	0.23(5)		100(22)	
(2, 3, 4)	2108.6(2)[f]	2^+	124.10	1984.5(2)[g]	1.4(3)		100(21)	
		4^+	385.95	1722.8(1)[g]	0.5(1)		36(7)	
	2352.0(2)[f]	2^+	875.90	1477.2(1)[g]	0.72(13)		100(18)	
		3^+	1030.95	1322.0(1)[g]	0.42(8)		58(11)	

[a]Literature values for intensities are from the evaluated ^{168}Hf β^+/ϵ decay data of Ref. [12], except where noted.
[b]Spin assignment from γ-γ angular correlation data; see text.
[c]γ-ray line was observed in Ref. [13], but not in Ref. [14].
[d]Intensity from Ref. [13].
[e]Intensity from Ref. [14].
[f]Level was not previously reported [12].
[g]γ-ray line was not previously reported [12].
[h]Level assignment is tentative because only a single depopulating transition is observed.
[i]Placement of transition is tentative.
[j]Transitions from the closely spaced levels at 1797.2 and 1799.5 keV are most likely doublets. Each transition is assigned a primary placement as depopulating one of these levels on the basis of the transition energy measured in a gated spectra but may contain an unresolved contribution from the other depopulating member of the pair.

of solid angle correction, are given in Table III and are in good agreement with the theoretical values. The solid angle corrections were calculated by using the formalism given in Ref. [15].

In Table III, the experimental A_2 and A_4 coefficients are given for all the angular correlations measured in the present work. The data of Table III are also shown in Figs. 5 and 6, where the standard ellipses A_4 versus A_2 as a function of the $E2/M1$ mixing ratio δ are plotted for the relevant spin sequences. The values of the mixing parameter δ in Table III were determined by comparing the experimental correlation coefficients with the theoretical calculations for various values of δ, using the convention of Krane and Steffen [16].

A. Low-lying levels in ^{168}Hf

Many of the low-spin, nonyrast states reported [12] in ^{168}Hf have been observed only in prior β-decay studies. Leber *et al.* [13] used the same reaction as the present work to produce ^{168}Ta and then the He-jet technique to transport

TABLE III. Experimental coefficients A_2 and A_4 obtained in the present work from fits of the angular correlation data to the sum of Legendre polynomials $1 + A_2P_2(\cos\theta) + A_4P_4(\cos\theta)$ and the corresponding measured δ values. The values of A_2 and A_4 are corrected for solid angle attenuation.

Nucleus	Cascade (keV)	Spin sequence	A_2	A_4	δ[a]
^{168}Hf	262–124	$4_1^+ \to 2_1^+ \to 0_1^+$	0.104(10)	0.006(14)	$E2$
	818–124	$0_2^+ \to 2_1^+ \to 0_1^+$	0.33(3)	1.08(5)	$E2$
	752–124	$2_2^+ \to 2_1^+ \to 0_1^+$	−0.004(32)	0.29(4)	-10^{-9}_{+3}
	907–124	$3_1^+ \to 2_1^+ \to 0_1^+$	−0.14(3)	−0.12(3)	$+11^{+13}_{-4}$
	645–262	$3_1^+ \to 4_1^+ \to 2_1^+$	−0.021(37)	−0.22(4)	<-20 or >10
	673–262	$2_3^+ \to 4_1^+ \to 2_1^+$	0.19(2)	0.05(3)	$E2$
	935–124	$2_3^+ \to 2_1^+ \to 0_1^+$	0.022(42)	0.27(7)	-8^{-10}_{+4}
	775–262	$4_3^+ \to 4_1^+ \to 2_1^+$	−0.078(20)	0.046(20)	$+0.8^{+0.6}_{-0.4}$
^{166}Yb	228–102	$4_1^+ \to 2_1^+ \to 0_1^+$	0.104(20)	0.005(26)	$E2$
	832–228	$4_2^+ \to 4_1^+ \to 2_1^+$	0.019(15)	0.075(25)	$+0.6 \pm 0.2$
	997–228	$5_1^+ \to 4_1^+ \to 2_1^+$	−0.21(2)	−0.03(1)	-0.2 ± 0.1 or -10^{-13}_{+3}
^{168}Yb	896–88	$2_2^+ \to 2_1^+ \to 0_1^+$	0.027(28)	0.31(4)	-7^{-7}_{+2}
	780–199	$3_1^+ \to 4_1^+ \to 2_1^+$	−0.15(23)	−0.112(20)	-8^{-3}_{+2}
	885–199	$4_2^+ \to 4_1^+ \to 2_1^+$	−0.069(17)	0.14(2)	-6^{-2}_{+1}

[a]Convention of Krane and Steffen [16]; all mixing ratios are for the first transition in the respective cascade.

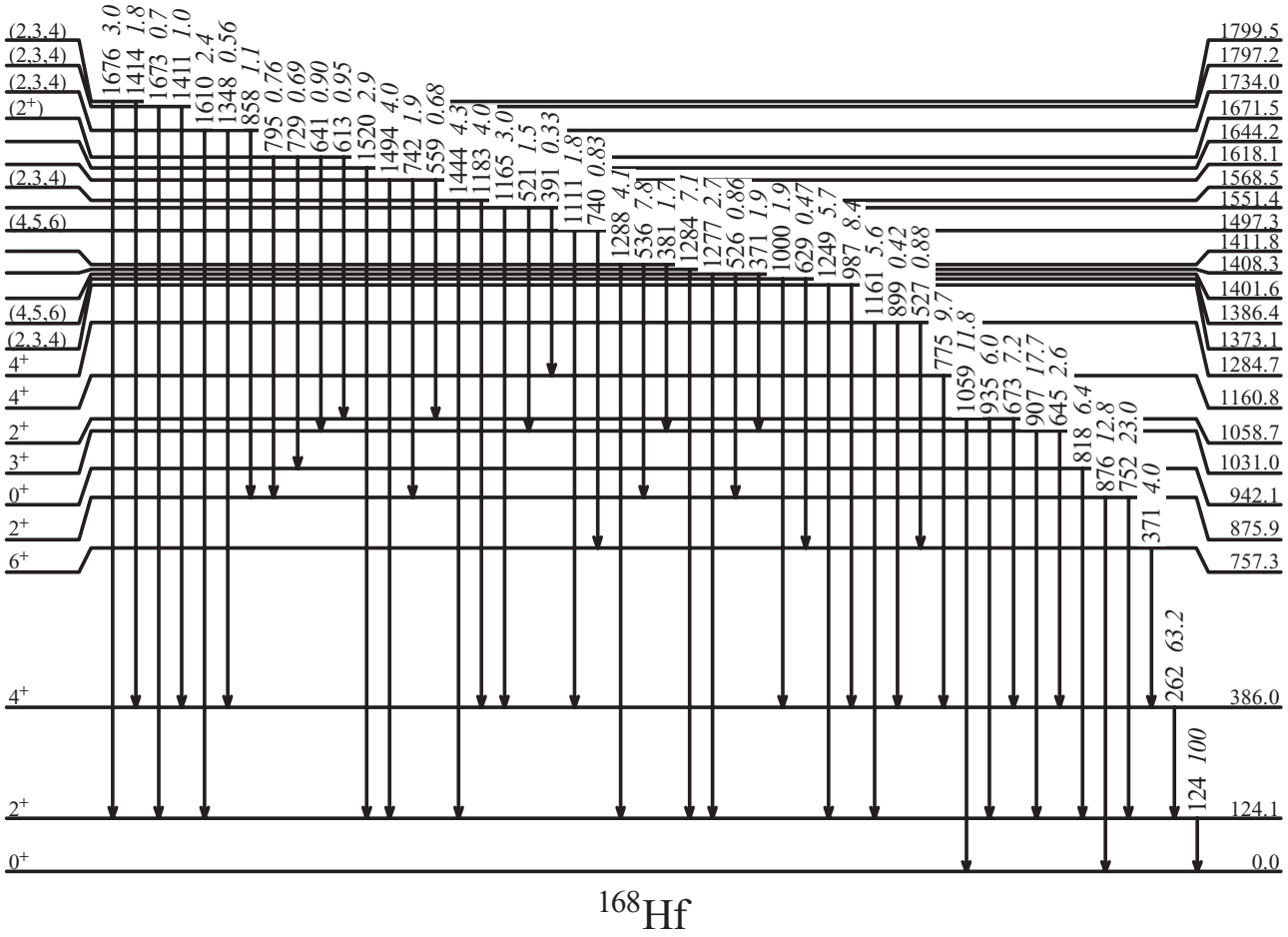

FIG. 3. Level scheme of ^{168}Hf populated in the β^+/ϵ decay of ^{168}Ta for levels below 1800 keV deduced in the present work. Levels are marked with their energy in keV. Transitions are labeled by their energy in keV and relative intensities (in β decay) in italics.

the activity to a detector area. Hild *et al.* [14] used the ^{133}Cs(^{40}Ar, 5n) reaction and a combination of He-jet and tape collector setups to study the decay of ^{168}Ta. The evaluated ^{168}Ta β-decay data of Ref. [12] is based primarily on the latter study [14]. The experimental results for levels of interest in the structural interpretation of ^{168}Hf are summarized in the following. Cases where the present measurement was able to resolve discrepancies between the results of the previous two β-decay studies are also described in detail.

The level at 876 keV was previously reported [12] to decay to the 2_1^+ level and 0_1^+ level through transitions of 752 and 876 keV, respectively, and tentatively assigned a J^π of 2^+. These two branches were observed and confirmed to have intensities consistent with those given in the literature. The angular correlation analysis of the 752-keV transition confirms the previous spin assignment of 2^+, as shown in Fig. 5. From the measured mixing ratio, the 752-keV, $2_2^+ \rightarrow 2_1^+$ transition was found to be predominantly $E2$ in character.

The level at 942 keV was previously reported [12] to decay to only the 2_1^+ level by a transition of 818 keV and tentatively assigned a J^π of 0^+. Analysis of the angular correlation data for the 818-keV transition confirms the 0^+ spin assignment, as shown in Fig. 4.

The level at 1031 keV was previously reported [12] to decay only to the 2_1^+ level by a transition of 907 keV and tentatively assigned a J^π of 3^+. A transition of 645 keV to the 4_1^+ state was reported by Ref. [13] with intensity 8.5(14). However, a 645-keV transition was not observed in a later study (Ref. [14]), where only an upper limit on the intensity of <3.0 is reported. In the present work, a 645.05(10)-keV transition with intensity 2.6(3) is observed to depopulate the level at 1031 keV. Evidence for the placement of this transition is given in Fig. 7. The 645-keV line is strongly coincident with the 262-keV, $4_1^+ \rightarrow 2_1^+$ transition, as shown in Fig. 7(a). In addition, a gate on the 521-keV transition populating the level at 1031 keV, as given in Fig. 7(b), clearly shows both the 907- and 645-keV depopulating transitions. The measured intensity of the 645-keV transition is consistent with the limit reported in Ref. [14], but it does not account for the large intensity reported in Ref. [13]. A significant amount of the singles intensity measured in the present work at this energy comes from a 645.24(3)-keV contaminant transition in ^{160}Dy [17] identified by its coincidences with the 86-, 197-, and

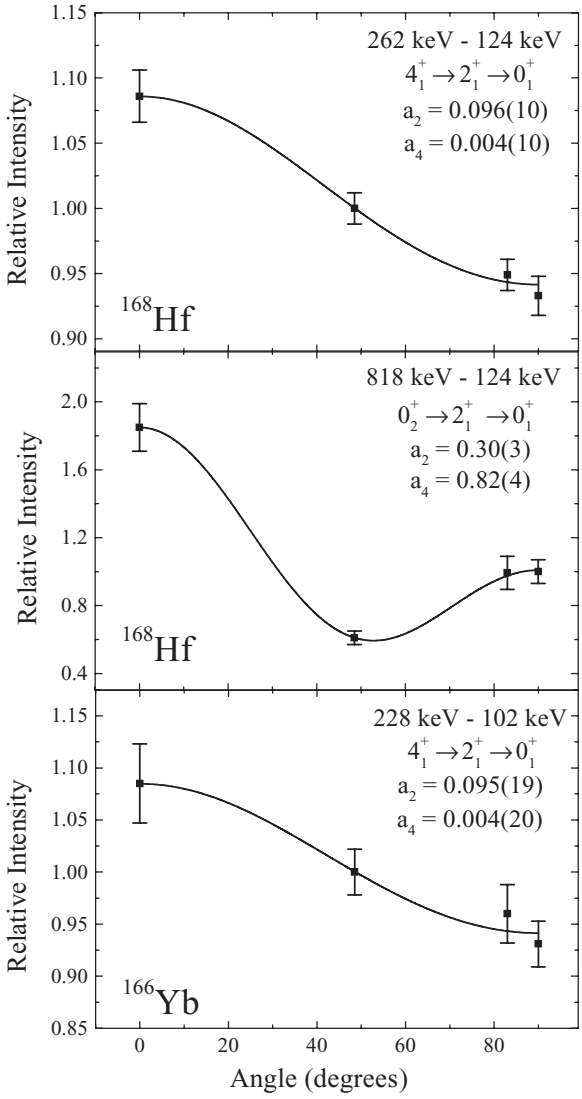

FIG. 4. Angular correlations for pure $E2$ cascades in ^{168}Hf and ^{166}Yb used to test the normalization procedure. The solid lines are fits to a sum of Legendre polynomials. The coefficients a_2 and a_4 are not corrected for solid angle attenuation.

962-keV transitions in that nucleus. Angular correlation analysis of both the 907- and 645-keV transitions (Figs. 5 and 6) confirms the 3^+ spin assignment. Both transitions were determined to be predominately $E2$ in character (Table III).

The level at 1161 keV was previously reported to decay by a single transition of 775 keV to the 4_1^+ state and tentatively assigned a J^π of 2^+. This transition was observed and confirmed to have an intensity consistent with the literature. The present angular correlation analysis determines the spin as $J = 4$, as shown in Fig. 6, with a strong $M1$ component for the 775-keV transition.

A level at 1216 keV was identified in β^+/ϵ decay [12] on the basis of a single depopulating transition of 831 keV to the 4_1^+ state with intensity 7.8(20). From spectra gated on the 262-keV, $4_1^+ \rightarrow 2_1^+$ transition, no coincidences are observed with an 831-keV transition, as shown in Fig. 8. Coincidence data established an 830-keV line and a 832-keV line as both

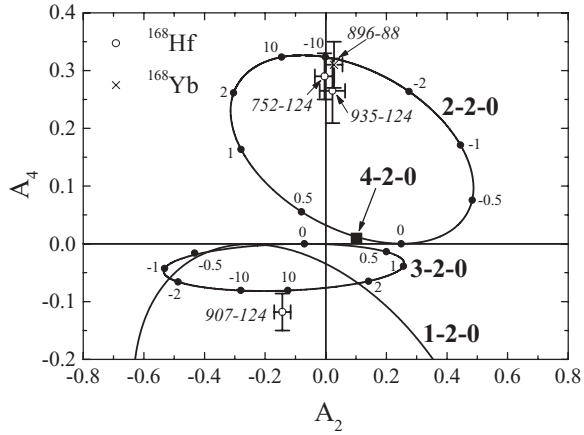

FIG. 5. Angular correlation ellipses A_4 vs A_2 for the spin sequences J–2–0, $J = 1, 2, 3, 4$ for the range $\delta = -\infty, +\infty$. The values of δ are labeled on the respective points on the ellipses. The experimental points correspond to the results of γ-γ angular correlations in ^{168}Hf and ^{168}Yb, labeled by their energy in italics.

belonging to the decay of ^{166}Lu to ^{166}Yb [18], produced in a competing reaction channel. Therefore, having found no support for the reported [12] transition depopulating the level at 1216 keV and with no observation of any direct or indirect population of the level, we conclude that there is no evidence for the existence of a level at 1216 keV.

The level at 1285 keV was previously proposed [12] to decay by a single transition of 1161 keV to the 2_1^+ level and tentatively assigned a J^π of 4^+. Two additional transitions were reported by Ref. [13], a 527-keV transition with intensity 7.3(8) and a 899-keV transition with intensity 5.4(11) to the 6_1^+ level and 4_1^+ levels, respectively. In the later β-decay study (Ref. [14]) these transitions were not observed, but upper limits for the 527- and 899-keV transitions of <2.5 and <3.7, respectively, were reported. In the present work, both the 527- and 899-keV transitions are observed to depopulate the level

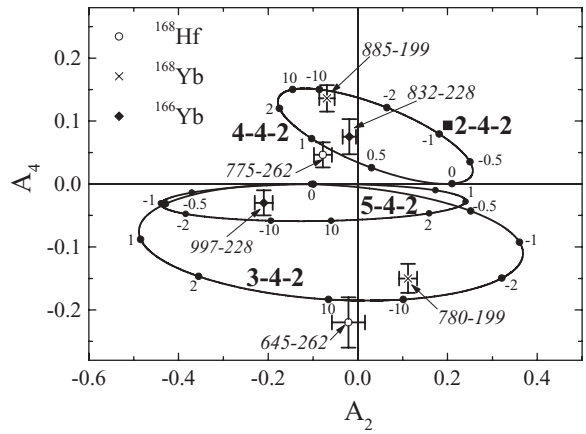

FIG. 6. Angular correlation ellipses A_4 vs A_2 for the spin sequences J–4–2, $J = 2, 3, 4, 5$ for the range $\delta = -\infty, +\infty$. The values of δ are labeled on the respective points on the ellipses. The experimental points correspond to the results of γ-γ angular correlations in ^{168}Hf and ^{166,168}Yb, labeled by their energy in italics.

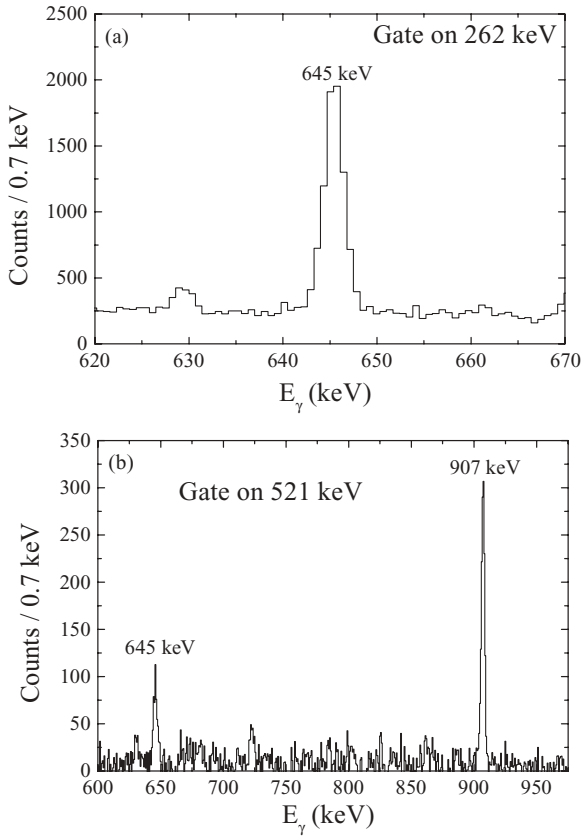

FIG. 7. Gated coincidence spectra giving evidence for the placement of the 645-keV transition. Spectra gated on (a) the 262-keV, $4_1^+ \rightarrow 2_1^+$ transition and (b) the 521-keV γ ray.

at 1285 keV. An 899-keV line is found in coincidence with the 262-keV, $4_1^+ \rightarrow 2_1^+$ transition as shown in Fig. 8. This confirms the placement of Ref. [13] with an 898.8(2)-keV line with intensity 0.42(8) populating the 4_1^+ state. As shown in Fig. 9(a), a 527-keV transition is observed in coincidence with the 371-keV, $6_1^+ \rightarrow 4_1^+$ transition. Similarly, a gate on the 527-keV transition is found to be coincident with transitions

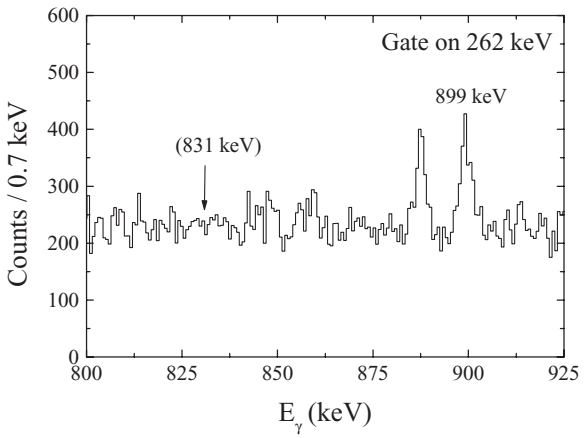

FIG. 8. Spectrum gated on the 262-keV, $4_1^+ \rightarrow 2_1^+$ transition showing the observed coincidence with an 899-keV transition and the unobserved coincidence with an 831-keV transition.

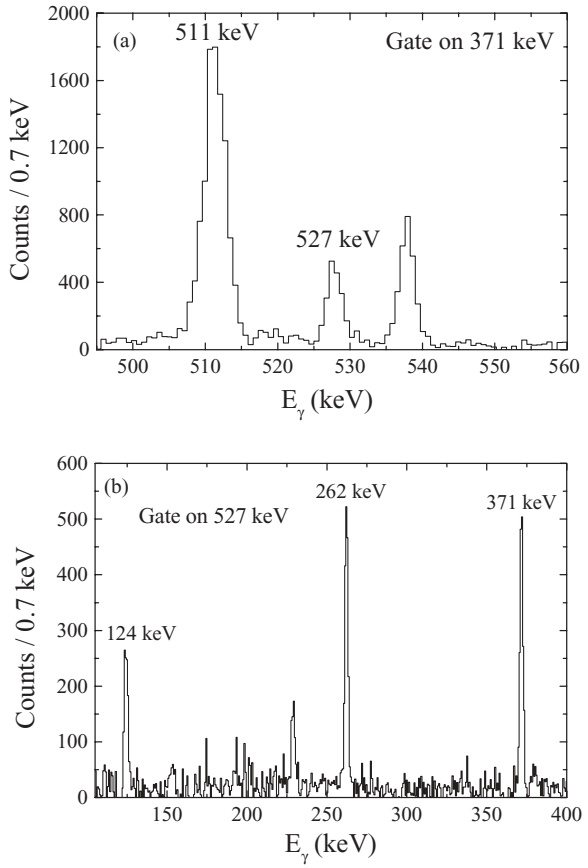

FIG. 9. Gated coincidence spectra providing evidence for the placement of the 527-keV transition. Spectra gated on (a) the 371-keV, $6_1^+ \rightarrow 4_1^+$ transition and (b) the 527-keV transition.

depopulating the 6_1^+, 4_1^+, and 2_1^+ levels, as shown in Fig. 9(b). This also confirms the original placement of Ref. [13] with a 527.4(1)-keV line with intensity 0.88(11) populating the 6_1^+ state. The measured intensities of the 527- and 899-keV transitions are consistent with the upper limits of Ref. [14], but they do not account for the large intensities reported in Ref. [13]. For the 527-keV transition, a significant amount of the singles intensity measured in the present work at this energy comes from a 526.01(10)-keV contaminant transition in ^{166}Yb [18]. For the 899-keV transition, no contaminant transition was observed at exactly this energy; however, a 896.12(5)-keV transition in ^{168}Yb was observed as a very strong line in the singles spectrum, which could have contributed to the strength observed in Ref. [13]. The observed depopulating transitions support the 4^+ assignment for this level.

In the present work, fifteen new levels are identified above 1300 keV (Table II). As an example of the level of support surrounding these new levels, the evidence for a selected new level is described in detail. The level at 1411.78(8) keV is identified on the basis of newly observed transitions of 381, 536, and 1288 keV to the 3_1^+, 2_2^+, and 2_1^+ levels, respectively. As shown in Fig. 10(a), a 1288-keV transition is observed in coincidence with the 124 keV, $2_1^+ \rightarrow 0_1^+$ transition. Support for the placement of a 536-keV transition as depopulating the level at 1412 keV is given in Fig. 10(b). A 536-keV

transition is observed in coincidence with both the 752- and 876-keV transitions depopulating the 2_2^+ level at 876 keV. Finally, support for a 381-keV transition populating the 3_1^+ level is given in Fig. 10(c). A 381-keV transition is observed in coincidence with both the 907- and 645-keV transitions, which depopulate the 3_1^+ level at 1031 keV.

B. Select angular correlations in ^{166}Yb and ^{168}Yb

We also performed γ-γ angular correlation measurements on strong, contaminant-free transitions in ^{166}Yb and ^{168}Yb. These results are included in Table III and Figs. 5 and 6. In each of these nuclei, the measured δ values are consistent with previous measurements of multipolarities from α_K values, but they now allow for a better determination of the extent of $E2/M1$ mixing.

In ^{166}Yb, the δ value measured in the present work of 0.6 ± 0.2 for the 832-keV, $4_2^+ \rightarrow 4_1^+$ transition is consistent with the reported $M1$ character from the measured α_K value [19]. Two possible values of δ were found for the 997-keV, $5_1^+ \rightarrow 4_1^+$ transition. Combining this information with the α_K measurement [19], which favors an $E2$ transition, suggests that the appropriate δ value is -10^{-13}_{+3}.

In ^{168}Yb, limits on the multipole mixing were previously determined [20,21] from measured α_K values. The present measured δ values are consistent with the previous limits. The 780-, 885-, and 896-keV transitions were determined to be predominantly $E2$ in character, consistent with the $M1$ limits given in Ref. [21] of <44%, 39%, and <39%, respectively.

III. DISCUSSION

The newly developed solutions for the geometric models, CBS and Davidson potential, provide simple, single-parameter descriptions of transitional to deformed nuclei. ^{168}Hf, with a ground-state $R_{4/2}$ of 3.11, lies in a transitional region outside of a well-deformed structure and therefore should provide a good testing ground for these models. In addition, the predictions of the two parameter models, the exactly separable Davidson and the interacting boson approximation model, are also compared to the data for ^{168}Hf.

Because these models give predictions for the excited $K = 0^+, 2^+$ sequences, it is first necessary to make assignments of the observed states to these sequences. The first excited 2^+ state at 876 keV is assigned as the bandhead of the $K = 2^+$ excitation. This leaves the 2^+ state at 1059 keV as the most likely candidate for the 2^+ member of the 0_2^+-band sequence.

The mostly likely candidate for the 4^+ member of the γ band is the level at 1161 keV, leaving the 4^+ level at 1285 keV as possibly the 4^+ member of the 0_2^+-band sequence. There are several supporting arguments for these assignments. From an energy standpoint, this assignment results in band structures appropriate for $K = 0^+$ and 2^+ excitations. The resulting $R_{4/2}$ ratio in the excited $K = 0^+$ band is 2.94. The energy staggering in the γ band is also sensitive to the nuclear shape [22]. A common measure of this is the quantity $S(4) \equiv [E(4_\gamma^+) - 2E(3_\gamma^+) + E(2_\gamma^+)]/E(2_1^+)$. For an axial rotor, $S(4) = +0.33$. For a γ-soft deformed structure

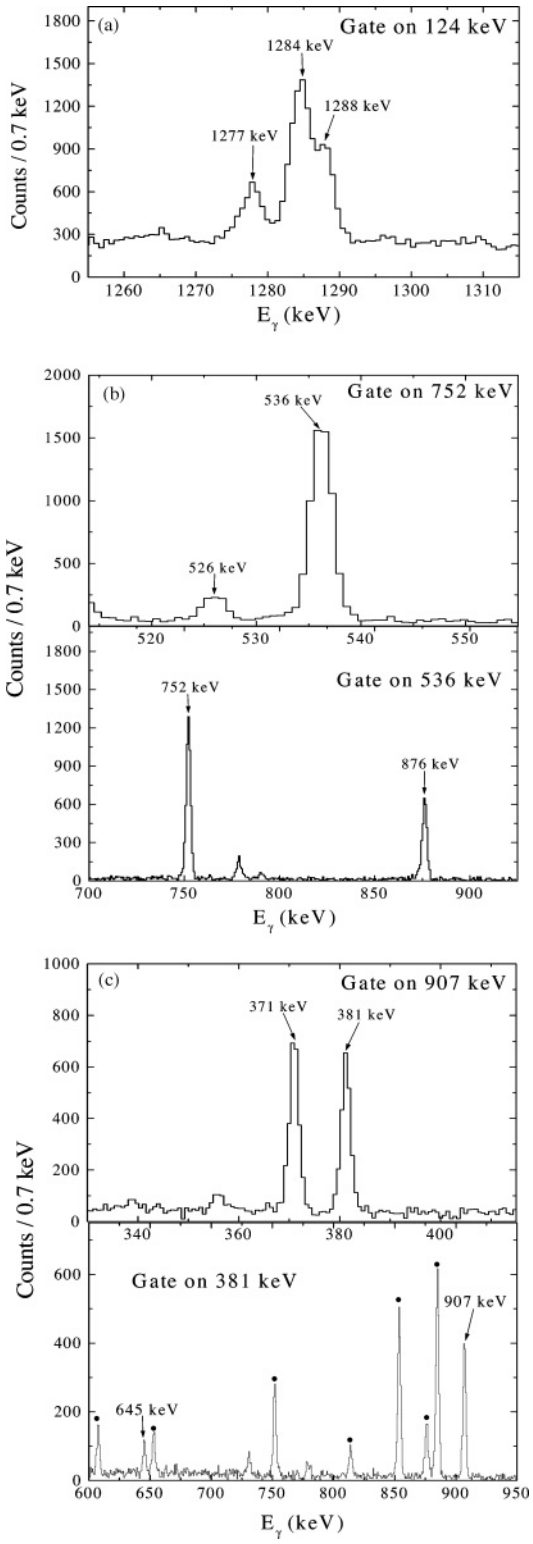

FIG. 10. Gated coincidence spectra providing evidence for a newly identified level at 1412 keV. (a) Spectrum gated on the 124-keV, $2_1^+ \rightarrow 0_1^+$ transition showing coincidences with a 1288-keV transition. (b) Spectra providing evidence for a new transition of 563 keV. (c) Spectra providing evidence for a new 381-keV transition; the solid circles correspond to transitions belonging to ^{168}Yb that originate from coincidences with a 380.01-keV transition in that nucleus [12].

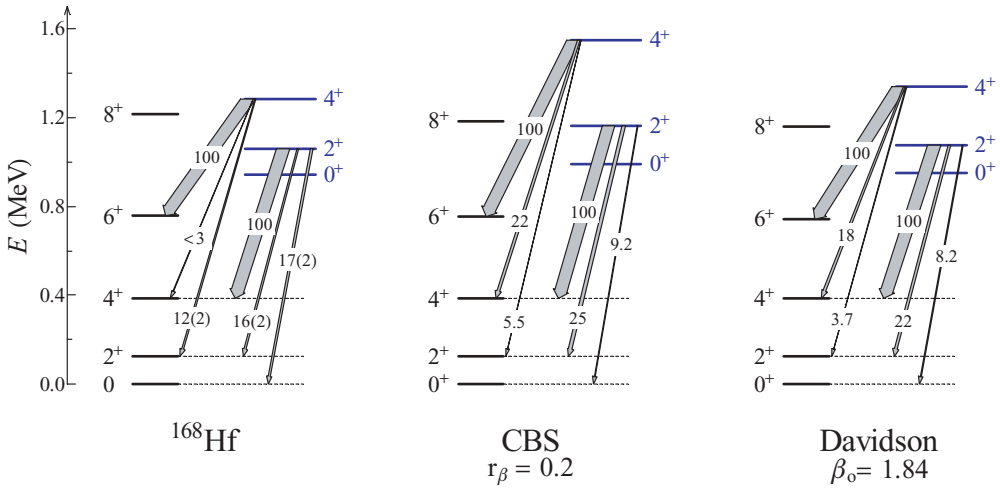

FIG. 11. (Color online) Experimental level scheme and relative $B(E2)$ strengths for ^{168}Hf (left) compared with the predictions for the CBS model (middle) and the Davidson potential (right). Energies are normalized to the experimental $E(2_1^+)$ value. $B(E2)$ values are normalized to the strongest branch with the strength indicated by the widths of the transition arrows.

$S(4) < 0$ whereas for a rigid triaxial rotor, $S(4) > 0.33$. This assignment leads to $S(4) = -0.20$. If the assignment of the 4^+ states is reversed, this results in an $R_{4/2}$ ratio in the excited $K = 0^+$ band of 1.9 and a staggering in the quasi-γ band of $S(4) = +0.80$. The first of these is well outside what would be expected for a well-deformed band structure and the second would be highly anomalous since the rare-earth region is well known to exhibit axially symmetric structures. The assignment of 4^+ states is also suggested by the $E2$ branching ratios. In the Alaga limit, the 4^+ of the $K = 0^+$ sequence is expected to have a strong transition to the 6^+ of the ground-state band. Indeed, the strongest $B(E2)$ from the level at 1284 keV populates the 6_1^+ level, whereas this transition is not observed from the level at 1161 keV.

Having assigned the $K = 0^+, 2^+$ excited sequences up through $J^\pi = 4^+$, we can now compare the level scheme of ^{168}Hf to the different model predictions. To fix the parameters of the CBS and the Davidson potential models, the single free parameter in each was varied to reproduce the $R_{4/2}$ ratio in ^{168}Hf. The corresponding parameters are $r_\beta = 0.20$ and $\beta_o = 1.84$ for the CBS and Davidson potential models, respectively. The resulting level schemes are compared with the data in Fig. 11. Even though the parameters were fixed based on the $R_{4/2}$ ratio alone, the agreement is excellent for the location of the first excited 0^+ state. The CBS and Davidson potential models predict $R_{0/2} = E(0_2^+)/E(2_1^+)$ ratios of 8.0 and 7.7, respectively, compared with the experimental value in ^{168}Hf of 7.6.

The $B(E2)$ transition strengths for the CBS and Davidson potential models are calculated by using the transition operators given in Refs. [5] and [7], respectively. The predicted branching ratios from the excited 0^+ sequence are almost identical for both models. The branching ratios from members of the 0_2^+ sequence are also summarized in Fig. 12. Both models provide a reasonable description for the decay of the 2^+ and 4^+ member of the 0_2^+ sequence. The only large discrepancy is in the $4_3^+ \rightarrow 4_1^+$ transition in which both models overpredict the data by almost an order of magnitude. Included in Fig. 12 are the Alaga ratios for axially symmetric well-deformed nuclei. The Alaga ratios differ noticeably from both the data and the predictions of the CBS model and Davidson potential model, significantly overpredicting the data. A summary of all theoretical $B(E2)$ transition strengths predicted by the CBS and the Davidson potential models between the low-lying states shown in Fig. 11 is given in Table IV. Again, the predicted transition strengths are very similar for both models.

The most obvious difference between the CBS and Davidson potential model predictions is in the spacings of the excited 0_2^+ sequence. The Davidson potential gives the very simple prediction that the inertial properties of the ground and 0_2^+ bands are identical; that is, the $R_{4/2}$ ratios are equal, regardless of the parameter β_o. This agrees well with the data on ^{168}Hf, where the $R_{4/2}$ ratios in the ground and 0_2^+ bands are

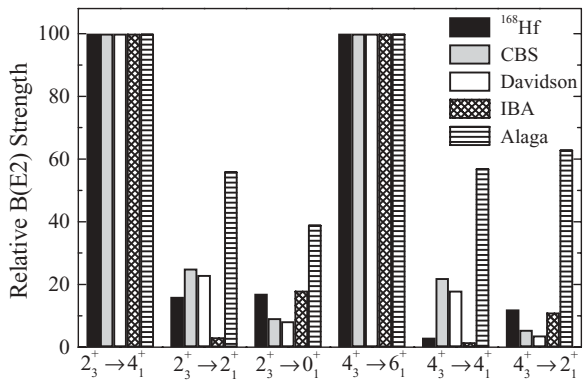

FIG. 12. Comparison of the relative interband $B(E2)$ values from levels belonging to the 0_2^+ sequence in ^{168}Hf with the predictions of the CBS model, the Davidson potential, IBA calculations, and the Alaga ratios. Theory and experiment are normalized to 100 for the strongest branch from the 4^+ and 2^+ levels.

TABLE IV. Theoretical $B(E2)$ strengths predicted by the CBS, Davidson potential, IBA, and ES-D from fits to the data on ^{168}Hf. Parameters for each model are included in the table and in the text. Transitions strengths are normalized to $B(E2; 2_1^+ \rightarrow 0_1^+) = 100$.

$B(E2; J_i^+ \rightarrow J_f^+)$	CBS $r_\beta = 0.2$	Davidson $\beta_o = 1.84$	IBA $\zeta = 0.70$ $\chi = -0.60$	ES-D $\beta_o = 0.0$ $c = 2.4$
$2_1^+ \rightarrow 0_1^+$	100	100	100	100
$4_1^+ \rightarrow 2_1^+$	153	154	145	152
$6_1^+ \rightarrow 4_1^+$	184	189	161	185
$8_1^+ \rightarrow 6_1^+$	211	226	167	218
$0_2^+ \rightarrow 2_1^+$	40	42	14	38
$2_{K=0}^+ \rightarrow 0_2^+$	90	132	57	130
$2_{K=0}^+ \rightarrow 0_1^+$	2.6	2.8	1.4	2.7
$2_{K=0}^+ \rightarrow 2_1^+$	6.8	7.4	0.23	6.9
$2_{K=0}^+ \rightarrow 4_1^+$	28	33	7.5	29
$4_{K=0}^+ \rightarrow 2_{K=0}^+$	126	196	84	192
$4_{K=0}^+ \rightarrow 2_1^+$	1.3	1.4	0.72	1.6
$4_{K=0}^+ \rightarrow 4_1^+$	5.5	6.8	0.01	6.3
$4_{K=0}^+ \rightarrow 6_1^+$	25	38	6.7	33
$2_\gamma^+ \rightarrow 0_1^+$			3.4	2.0
$2_\gamma^+ \rightarrow 2_1^+$			18	3.1
$2_\gamma^+ \rightarrow 4_1^+$			0.06	0.17
$3_\gamma^+ \rightarrow 2_1^+$			7.1	3.8
$3_\gamma^+ \rightarrow 4_1^+$			9.9	1.7
$3_\gamma^+ \rightarrow 2_\gamma^+$			106	233
$4_\gamma^+ \rightarrow 2_\gamma^+$			64	66
$4_\gamma^+ \rightarrow 2_1^+$			0.34	1.3
$4_\gamma^+ \rightarrow 4_1^+$			16	4.1
$4_\gamma^+ \rightarrow 6_1^+$			0.12	0.40

3.11 and 2.94, respectively. The CBS model, however, predicts that the 0_2^+ band is more deformed than the ground-state band. For the r_β value used in the present fit, the CBS model gives an $R_{4/2}$ ratio in the 0_2^+ band of 3.25. In addition to this discrepancy, the overall spacing in the 0_2^+ sequence given by the CBS model is much more expanded than what is observed in ^{168}Hf. This points to an interesting feature of the CBS model. The predicted $R_{4/2}$ in the 0_2^+ sequence suggests a more deformed structure for this band compared with the ground-state band. However, the 2^+–0^+ spacing predicted by the CBS model suggests a less deformed structure. In the case of the fit to ^{168}Hf, the CBS model gives the 2^+–0^+ spacing in the excited 0^+ band as 170 keV, compared with the ground-state 2^+–0^+ spacing of 124 keV.

The flexibility in describing ^{168}Hf can be increased by considering potentials with additional free parameters. For this purpose, the level scheme of ^{168}Hf is also compared to the predictions of the ES-D model and the IBA. Both of these models also include predictions for the γ band. The two free parameters for each of these models were chosen with an equal emphasis on reproducing the $R_{4/2}$ ratio, as well as the energies of the 0_2^+ and 2_γ^+ levels.

For the IBA description, calculations were performed using the Hamiltonian [23]

$$H(\zeta, \chi) = a\left[(1-\zeta)\hat{n}_d - \frac{\zeta}{4N_B}\hat{Q}^\chi \cdot \hat{Q}^\chi\right], \qquad (4)$$

where $\hat{n}_d = d^\dagger \cdot \tilde{d}$ and $\hat{Q}^\chi = (s^\dagger \tilde{d} + d^\dagger s) + \chi(d^\dagger \tilde{d})^{(2)}$. Electromagnetic transitions are calculated using the $E2$ operator, $T(E2) = e_B Q$. The two free parameters are ζ and χ, and $N_B = 12$ is the number of valence bosons. A reasonable description of ^{168}Hf was obtained with the parameters $\zeta = 0.70$ and $\chi = -0.60$. The scaling factor a used in the present fit was 1.13. Calculations were performed by diagonalizing the Hamiltonian numerically using the computer code PHINT [24].

The parameters for the ES-D potential that best reproduce the structure of ^{168}Hf are $\beta_o = 0$ and $c = 2.4$. At first, these might seem contradictory to the parameters chosen for the Davidson potential, where a value of $\beta_o = 1.84$ was used. The potential for the exactly separable case can be written as

$$V(\beta, \gamma) = \beta^2 + \frac{\beta_o^4}{\beta^2} + \frac{(3c)^2\gamma^2}{\beta^2} = \beta^2 + \frac{\beta_o^4 + (3c)^2\gamma^2}{\beta^2} \qquad (5)$$

and thus the predictions for the ES-D model depend on the parameter combination of β_o and c. The energy of the γ band is most sensitive to the parameter c, as might be expected since c is a measure of the stiffness of the potential in γ. Incorporating a finite value of c to reproduce the energy of the γ bandhead then requires a smaller value of β_o since the potential is already driven to increased stiffness by a nonzero c term.

The resulting predictions for both the ES-D model and the IBA along with the level scheme of ^{168}Hf are given in Fig. 13. The energies of the 0_2^+ and 2_γ^+ levels are reasonably well reproduced by both the ES-D model and the IBA, with the IBA giving a slightly better fit to the 0_2^+ energy. The predictions for relative $B(E2)$ strengths are almost identical for the ES-D model compared with the Davidson potential described earlier. Overall, the IBA gives a very good description of the $B(E2)$ strengths from both the $K = 0^+$ and 2^+ excited bands. As seen in Fig. 13, with the exception of the $2_3^+ \rightarrow 2_1^+$ transition, the IBA calculations reproduce almost exactly the transition strengths observed in ^{168}Hf. Table IV includes a more complete summary of theoretical $B(E2)$ transition strengths predicted by the IBA and ES-D model.

The spacing in the 0_2^+ sequence is again reproduced more closely by the Davidson potential. The IBA predicts a much less deformed structure for the 0_2^+ band, with $R_{4/2} = 2.33$. Unlike the CBS model, the predictions for the structure of the 0_2^+ sequence are consistent, with both the $R_{4/2}$ value and the 2^+–0^+ spacing in the excited band suggesting structure that is less deformed than the ground-state band. This is supported also by the quadrupole moments given in the IBA calculation, with the 2^+ state of the 0_2^+ sequence predicted to have a quadrupole moment ~70% that of the ground state 2^+.

Although each of these models would seem to have similar character (e.g., soft potentials in β for transitional nuclei and axially symmetric shapes) the differences for some observables are striking. It is an interesting challenge to try to understand these differences and their origin. For the observables discussed here, the Davidson potential provides the best description of the low-lying $K = 0^+, 2^+$ excitations in ^{168}Hf. The disagreements with the structure of the excited $K = 0^+$ sequence given by the CBS model can be attributed to the infinite rigidity of the outer wall used in the potential. Thus,

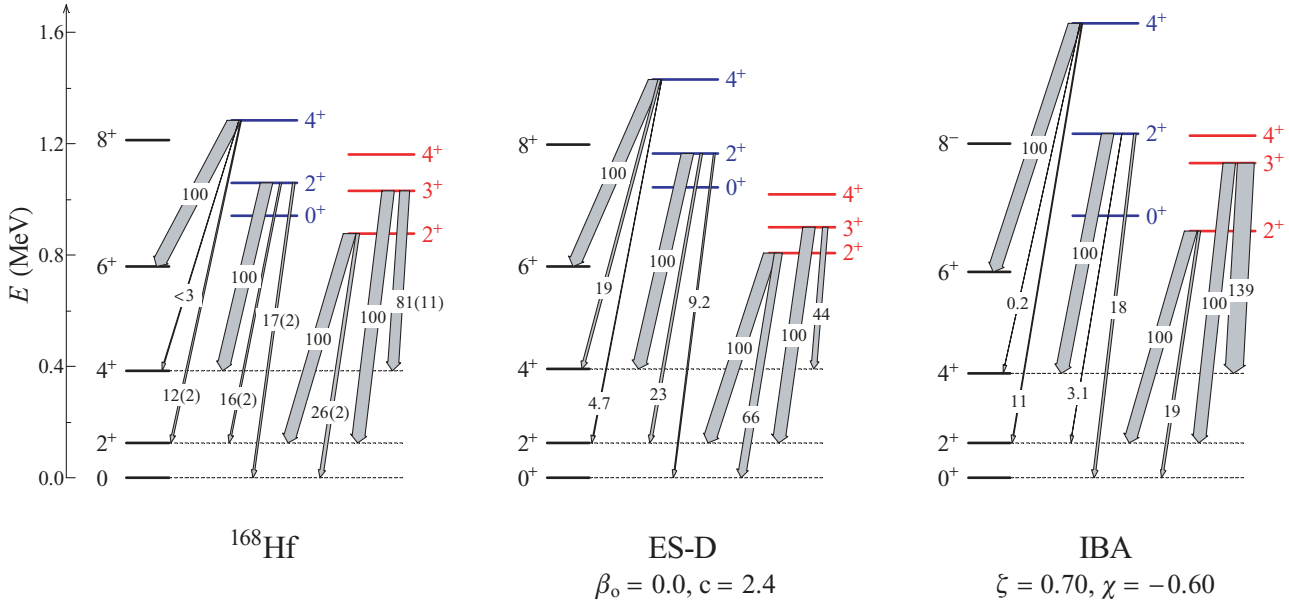

FIG. 13. (Color online) Experimental level scheme and relative $B(E2)$ strengths for ^{168}Hf (left) compared with the predictions for the ES-D model (middle) and IBA calculations (right). Energies are normalized to the experimental $E(2_1^+)$ value. $B(E2)$ values are normalized to the strongest branch with the strength indicated by the widths of the transition arrows.

the softer outer wall of the potential given by the Davidson potential seems more realistic for describing transitional nuclei. The reason behind the discrepancy in the IBA predictions for the structure of the excited $K = 0^+$ sequence remains an open question. For $E2$ transitions, the nature of the transition operator itself may play an important role.

IV. CONCLUSIONS

Off-beam, γ-ray spectroscopy was performed on ^{168}Hf populated in β^+/ε decay. New coincidence data provided a significantly revised level scheme, and γ-γ angular correlation measurements yielded spin and multipolarity information on important states and transitions. The resulting level scheme was compared with the predictions of new geometrical models as well as with predictions of the IBA. Overall, the best description of both level energies and $E2$ transition strengths is obtained with a Davidson potential in the β degree of freedom.

ACKNOWLEDGMENTS

Valuable discussions with D. Bonatsos, D. Lenis, D. Petrellis, and N. Pietralla are acknowledged. This work was supported by U.S. DOE Grant No. DE-FG02-91ER-40609.

[1] F. Iachello and A. Arima, *The Interacting Boson Model* (Cambridge University Press, Cambridge, 1987).
[2] G. Gneuss, U. Mosel, and W. Greiner, Phys. Lett. **B30**, 397 (1969).
[3] G. Gneuss, U. Mosel, and W. Greiner, Phys. Lett. **B31**, 269 (1970).
[4] G. Gneuss and W. Greiner, Nucl. Phys. **A171**, 449 (1971).
[5] N. Pietralla and O. M. Gorbachenko, Phys. Rev. C **70**, 011304(R) (2004).
[6] P. M. Davidson, Proc. R. Soc. London, Ser. A **135**, 459 (1932).
[7] Dennis Bonatsos, D. Lenis, N. Minkov, D. Petrellis, P. P. Raychev, and P. A. Terziev, Phys. Rev. C **70**, 024305 (2004).
[8] Dennis Bonatsos, E. A. McCutchan, N. Minkov, R. F. Casten, P. Yotov, D. Lenis, D. Petrellis, and I. Yigitoglu, Phys. Rev. C (in press).
[9] A. Bohr, Mat. Fys. Medd. K. Dan. Vidensk. Selsk. **26**, No. 14 (1952).
[10] F. Iachello, Phys. Rev. Lett. **87**, 052502 (2001).
[11] C. W. Beausang *et al.*, Nucl. Instrum. Methods Phys. Res. A **452**, 431 (2000).
[12] V. S. Shirley, Nucl. Data Sheets **71**, 261 (1994).
[13] R. E. Leber, P. E. Haustein, and I.-M. Ladenbauer-Bellis, J. Inorg. Nucl. Chem. **38**, 1591 (1976).
[14] T. Hild, W.-D. Schmidt-Ott, V. Freystein, F. Meissner, E. Runte, H. Salewski, and R. Michaelsen, Nucl. Phys. **A492**, 237 (1989).
[15] D. C. Camp and A. L. Van Lehn, Nucl. Instrum. Methods **76**, 192 (1969).
[16] K. S. Krane and R. M. Steffen, Phys. Rev. C **2**, 724 (1970).
[17] C. W. Reich, Nucl. Data Sheets **105**, 557 (2005).
[18] E. N. Shurshikov and N. V. Timofeeva, Nucl. Data Sheets **67**, 45 (1992).
[19] C. A. Fields, K. H. Hicks, and R. J. Peterson, Nucl. Phys. **A431**, 473 (1984).
[20] A. Charvet, R. Duffait, A. Emsallem, and R. Chéry, Nucl. Phys. **A156**, 276 (1970).
[21] V. Barci, G. Ardisson, D. Trubert, and M. Hussonnois, Phys. Rev. C **60**, 024304 (1999).
[22] N. V. Zamfir and R. F. Casten, Phys. Lett. **B260**, 265 (1991).
[23] V. Werner, N. Pietralla, P. von Brentano, R. F. Casten, and R. V. Jolos, Phys. Rev. C **61**, 021301(R) (2000).
[24] O. Scholten, KVI-63, Groningen (unpublished).